Analyst

PAPER

View Article Online
View Journal | View Issue

Cite this: *Analyst*, 2017, **142**, 3219

Spatially offset Raman spectroscopy for photon migration studies in bones with different mineralization levels

Kay Sowoidnich, *[a,b] John H. Churchwell,[b] Kevin Buckley,[a,b] Allen E. Goodship,[b] Anthony W. Parker[a,b] and Pavel Matousek[a,b]

The ability of Spatially Offset Raman Spectroscopy (SORS) to obtain chemically specific information from below the sample surface makes it a promising technique for non-invasive *in vivo* diagnosis of bone conditions by sampling bone through the skin. The depth below a surface interrogated by SORS depends on the system's optical properties and is difficult to estimate for complex bone material. This paper uses 830 nm laser excitation to investigate the influence of bone mineralization on photon migration properties in deer antler cortex, equine metacarpal cortex and whale tympanic bulla. Thin slices form each type of bone (thickness: 0.6–1.0 mm) were cut and put together on top of each other forming stacks with a total thickness of 4.1–4.7 mm. A 0.38 mm thin slice of polytetrafluoroethylene (PTFE) served as a test material for Raman signal recovery and was placed in between the individual bone slices within the stack. At SORS offsets of 8.0–9.5 mm Raman bands of materials not present in healthy bone (*e.g.* PTFE as an example) can be recovered through 4.4–4.7 mm of cortical bone tissue, depending on mineralization level and porosity. These findings significantly increase our understanding of SORS analysis through bones of different composition and provide information that is vital to determine the value of SORS as a medical diagnostic technique. The data serve to define which SORS offset is best deployed for the non-invasive detection of chemically specific markers associated with infection, degeneration and disease or cancer within bone.

Received 8th March 2017,
Accepted 21st July 2017

DOI: 10.1039/c7an00408g

rsc.li/analyst

1. Introduction

Raman spectroscopy is an important analytical tool that provides chemically specific information but in opaque solids it is limited to the analysis of the surface layers. Spatially offset Raman spectroscopy (SORS) provides a means to obtain subsurface Raman spectra permitting full chemical characterization at differing depths below the surface of turbid samples. SORS continues to be developed and is used in a multitude of applications.[1] The concept behind SORS is that there is a spatial separation between the point of laser illumination and the point of Raman signal collection on the sample surface. This can be achieved in different sample illumination and Raman collection configurations, *e.g.* using specialized optical elements,[2] fiber optic probes,[3] or digital micro-mirror devices.[4] The depth from which the signals are obtained depends on the distance between the light delivery and collection points. Larger spatial separations favor the interrogation of deeper layers but there is also a dependence on the scattering properties of the sample.

SORS has proven to be particularly advantageous in the biomedical area,[5] *e.g.* for non-invasive quality assessment of red blood cells within sealed PVC bags.[6] In this domain, near infrared excitation wavelengths are generally very beneficial as fluorescence interference is significantly reduced and large accessible depths can be achieved due to low absorption of biological samples present in a part of this spectral region.[7,8] Often SORS spectra can be retrieved through several millimeters of diffusely scattering media. Current areas of active research using SORS include the detection of tumors,[9,10] the characterization of bone tissue engineering scaffolds[11] and the assessment of bone fracture healing.[12] Furthermore, the identification of potential bone disease markers[13–15] and the detection of abnormal bone formation in soft tissue[16] has been addressed. Several investigations have been conducted with different SORS illumination and collection geometries[17–19] and bone Raman spectra have been retrieved successfully through 3–5 mm of overlaying soft tissue.[20] The

[a]*Central Laser Facility, Research Complex at Harwell, STFC Rutherford Appleton Laboratory, Harwell Campus, Didcot OX11 0QX, UK. E-mail: kay.sowoidnich@stfc.ac.uk; Tel: +44 (0)1235-446416*
[b]*UCL Institute of Orthopaedics and Musculoskeletal Science, Royal National Orthopaedic Hospital, London HA7 4LP, UK*

potential of SORS for the *in vivo* detection of pathological bone has recently been demonstrated in the case of the genetic condition *osteogenesis imperfecta*.[21]

Despite these promising results there are major barriers to the clinical translation of the SORS technique. A key issue, and one we seek to address in this paper, is associated with questions regarding the depth Raman spectra are being recovered from for a particular sample at a given spatial offset. For bone, the subject of this paper, to date there is only limited information available about where within the bone the signal originates. It would be expected that the optical properties of bone material are related to the tissue composition and in order to get a more detailed insight into photon migration our group has conducted studies on cortical long bones[22,23] and preliminary investigations on highly mineralized bone tissue.[24] We have now significantly expanded on our preliminary work using SORS offsets of up to 9.5 mm to assess photon migration properties and Raman signal recovery from depth within three selected bone types. Beside typical long bone tissue the specimens comprise two types of bone (antler and bulla respectively) that exhibit amongst the lowest and highest mineralization levels in nature.

2. Materials and methods

2.1 Bone specimens

All bones have evolved and adapted for a specific function and their composition reflects adaptation for that particular purpose during evolution.[25] In this study we used an equine metacarpus as an example of a typical long bone resisting torsion and bending during locomotion, a deer antler as an example of a significantly less mineralized bone, adapted for toughness and fracture resistance in fighting and a tympanic bulla from a whale as an example of a highly mineralized bone, optimized for sound transmission. These samples cover a wide range of the mineralization levels that can be found in bone.

A cannon bone (third metacarpal bone) from a mature thoroughbred racehorse (obtained from an equine abattoir) was excised, separated from the remaining soft tissue using a scalpel, wrapped in Clingfilm, and fresh frozen in a −20 °C freezer. Before the cutting procedure the bone was allowed to thaw at ambient temperature (20 °C). From the metacarpus two sections with a length of 4 cm each were cut from the metaphysis (the end-shaft) with the cutting direction perpendicular to the long axis of the bone.[22] After an initial cut along the long axis of the bone the outermost slices from both sections with an approximate thickness of 2 mm each were discarded due to their natural curvature. Subsequently, seven thin slices of cortical bone with thickness 600 ± 30 μm (average ± standard deviation) were cut from these two sections using a high precision diamond-edged band-saw (EXAKT 300, EXAKT Advanced Technologies GmbH, Germany).

The antler bone (obtained from a red deer from a commercial deer farm in SW England) was processed in a similar way to the equine metacarpal. Two sections with a length of 4 cm each were cut from a standard site at the base of the antler, *i.e.* near the point where it is attached to the skull of the deer and seven slices of cortical bone with a thickness of 670 ± 50 μm were cut (the cutting direction was parallel to the long axis of the sections/organ).

The tympanic whale bulla (kindly provided by Prof. John Currey, University of York, UK) was cut in half at the center with the cutting direction perpendicular to the long axis of the bone. Using the same cutting direction, four slices with a thickness of 1030 ± 30 μm were cut. In this case, the slices were thicker because the highly mineralized bulla bone is very brittle and attempts to cut thinner slices were not successful.

Following the cutting of the samples, the individual slices and the remaining part of the bone section from which they were cut (hereafter named the "bone segment") were thoroughly rinsed with tap water. The specimens of metacarpal and antler were held in a plastic container filled with tap water to prevent dehydration and stored in a refrigerator at 5 °C. Owing to the fact that the bulla bone was already in a dry state before cutting and due to its intrinsically much lower water content compared to antler and long bones,[26] the whale bulla samples were kept dry, wrapped in Clingfilm and stored at room temperature. Before spectroscopic analysis all samples were allowed to equilibrate at ambient temperature for one-hour prior to data collection.

2.2 Spatially offset Raman spectroscopy instrument

A custom built instrument (Cobalt Light Systems Ltd, Oxfordshire, UK) based on the inverse SORS technique[2,27] was used to conduct the Raman measurements. To minimize fluorescence interference and to exploit low absorption of biological tissue in this spectral region the excitation wavelength used was 830 nm. The near-infrared diode laser delivers an annular illumination zone (ring thickness: 1 mm) with an optical power of 330 mW at the sample position. While the laser excitation ring has a selectable radius to adjust the spatial offset the signal collection zone is located at the center of the illumination ring in all cases.[2] In this study, the spatial offsets between excitation and collection areas were selected from 0 mm to 9.5 mm in increments of 0.5 mm.

The scattered radiation emerging from the collection zone (*ca.* 1.5 mm diameter) was spectrally filtered and only the Raman-shifted components were imaged onto a low-loss Optran WF fiber bundle (CeramOptec, East Longmeadow, MA). The fiber bundle is connected to a spectrograph (Raman Explorer, Headwall, MA) with attached CCD detector (Andor iDus 420 BR-DD; Andor, Belfast, Northern Ireland) providing a spectral resolution of 8 cm^{-1}. Additional information about this SORS instrument is available from our earlier publications.[20,28]

2.3 Photon migration assessment

For the investigation of photon migration properties inside the different types of bone individual slices of each species were put together forming stacks of 7 layers (equine metacarpal and

deer antler) and 4 layers (whale bulla). The total stack thickness was 4.17 mm, 4.69 mm and 4.12 mm for metacarpal, antler and bulla, respectively. Results of our previous work on photon migration[23] indicated that a diffuse scattering material beneath the actual depth inside the bone probed by SORS is essential for the effective return of photons, *i.e.* the target region needs to be surrounded by a diffusely scattering medium. When selecting a target depth at or close to the bottom of the stacks of bone slices this condition would not be met without additional material being present underneath. To account for this effect, in the present study the stacks of bone slices were put on top of the corresponding bone segments to allow for efficient signal recovery for all investigated depths. During the measurements, the samples of antler and metacarpal were kept moist while the bulla bone was kept in a dry state (owing to its much lower water content[26]).

To determine the depth inside the bone tissue from which the detected Raman signal originated, a 380 μm thin slice of polytetrafluoroethylene (PTFE) was used as reference material. It was first inserted on top; then between the bone slices of the stack as well as below the stack (*i.e.* immediately above the bone segment). PTFE was chosen for this purpose because it has a pronounced Raman band at 734 cm^{-1} separated and well resolved from all major bone signals. Furthermore, the signal strength of that characteristic PTFE band is of the same order of magnitude as the main bone phosphate signal at 961 cm^{-1}. For each investigated depth of the PTFE layer three randomly selected lateral positions on the sample surface were probed. At each spot 30 s spectra were collected, composed of 300 × 0.1 s accumulations in the case of metacarpal and antler. Due to very strong fluorescence from the bulla bone, causing the CCD detector to saturate at 0.1 s integration time, 500 × 0.06 s accumulations were recorded in this case, keeping the total acquisition time constant.

2.4 Data analysis

Before analysis, the spectra were multiplied by a correction function (obtained by means of a luminescent green glass standard) to correct for the sensitivity variation across the CCD, *i.e.* eliminating artifacts due to filter effects and CCD etaloning. The band intensities and ratios of the prominent bands of PTFE (C–F and C–C symmetric stretch at 734 cm^{-1})[29] and bone (phosphate symmetric stretch at 961 cm^{-1})[18] were calculated using Microsoft Excel (Microsoft, Redmond, WA) as described previously.[23] Calculations of the PTFE signal-to-noise (S/N) ratio involved the background noise value as determined in the spectral range from 660 cm^{-1} to 710 cm^{-1}, which is free from Raman signals of both PTFE and bone. A Gaussian distribution was fitted to the PTFE to bone Raman intensity ratios dependent on SORS offset to determine the offset which gives the maximum PTFE signal for a specified depth. To calculate signal recovery depths the PTFE S/N ratio in dependence of the depth of the PTFE slice inside the bone stack (corresponding to the overlaying bone thickness) was fitted using an exponential function. Uncertainties were estimated using the standard deviation of the three repeat measurements probed for each depth of the PTFE slice inside the bone stacks. The entire data fitting was performed using Matlab R2013a in conjunction with Ezyfit Toolbox.

3. Results and discussion

3.1 Bone material properties

The variations in composition are associated with differences in biological function of the selected bones.[30] The antler needs to be tough as it is used to fight other male deer and the selection pressure for stiffness is not great. In this case, selection rather strives for toughness to avoid brittle fracture ultimately resulting in a bone with high collagen content (*i.e.* low mineralization). For the metacarpal bone, stiffness (related to energy efficiency, a muscle wastes energy if a bone bends excessively) is the main driver of the composition but the organ cannot get too stiff or it will be susceptible to fracture. The bulla bone serves as a sound conductor and therefore a large stiffness (*i.e.* high mineralization) is favorable.

To quantify the compositional differences of the bone samples, two Raman peak ratios were taken. Firstly, the intensity of the bone phosphate band at 961 cm^{-1} divided by the intensity of the CH_2 deformation band at 1450 cm^{-1} (mineralization ratio), and secondly the intensity ratio of the bone phosphate band at 961 cm^{-1} to the bone carbonate band at 1071 cm^{-1} (carbonate substitution) were calculated. For comparison, also the density and porosity values of the bone specimens were compiled from the literature[30–33] and all results are shown in Table 1.

As expected,[28] the bones showed pronounced differences with respect to their mineralization ratio and the antler had the lowest value. The ratios determined for the metacarpal and the bulla were larger by a factor of 1.5 and 14, respectively. Regarding the carbonate substitution, the bulla exhibited the largest value here as well. However, not the antler as least mineralized bone but the metacarpal bone had the lowest carbonate substitution ratio. The maximum variation between lowest and highest carbonate substitution is 28% in this case.

The optical properties of bone are influenced by its density and porosity as well. The trend for the material density follows the trend for the mineralization, *i.e.* antler having the smallest

Table 1 Material characteristics of bone samples investigated in this study. Raman band intensity ratios are given as mean ± SD. The values for density,[30,31] and porosity,[32,33] (given in italics) are compiled from available literature data

	Deer antler	Equine metacarpal	Whale bulla
Phosphate to CH_2 deformation Raman intensity ratio	4.86 ± 0.06	7.39 ± 0.09	68 ± 7
Phosphate to carbonate Raman intensity ratio	5.3 ± 0.3	4.60 ± 0.08	5.87 ± 0.07
Density/g cm^{-3}	*1.86–1.89*	*2.06–2.20*	*2.47–2.49*
Porosity/%	*2.2–19.3*	*3.3–5.8*	*1.9–4.0*

density and bulla being the densest material with a variation of 34% between them. On average, the metacarpal is slightly (1.6%) more porous than the bulla but both types of bone tissue have comparable values for porosity. For the antler, however, the reported porosity covers a wide range up to almost 20%. The literature directly comparing antler and typical long bones is quite ambiguous regarding the porosity ratios between these two types of bone. Currey[32] reported average porosities of 4.55% for long bone and 16.35% for antler (ratio: 3.59) while Chen *et al.*[34] found porosities of 5.1% for long bone and 9.1% for antler (ratio: 1.78). As one single type of bone cannot be partially demineralized[35] one potential way to eliminate, or at least reduce, this difference in porosity would be to grind the bone tissue with different mineralization levels down to the same grain size – followed by compression into discs of defined thickness. This approach would overcome the issue of varying porosity but is less clinically relevant than using intact bone tissue as it would destroy the complexity of the bone micro-structure from which the optical scattering is likely to occur (*e.g.* the lamellae).

It has been reported that the cortical porosity of antlers varies along the main shaft with the lowest values found near the proximal end (*i.e.* close to the antler base).[33,36] Furthermore, there are significant differences in porosity of antler cortex between free-ranging deer (10.5%) and animals kept in the controlled environment of a deer farm (2.2%).[33] To account for the effect of porosity and to minimize its influence on our experiments, we therefore acquired an antler bone from a deer farm and selected a sample position next to the base of the antler. For our study we can summarize that potential differences in photon migration properties between bulla and metacarpal are likely, to a large extent, attributable to differences in their mineralization while for the more porous antler bone the lower mineralization may not be the only contributing factor.

3.2 PTFE signal recovery of buried PTFE layer

Representative SORS spectra of the three different bone types with the PTFE layer placed at depths of 4.0–4.2 mm inside the bone tissue, recorded at 0 mm offset and 9 mm offset, are displayed in Fig. 1. The spectra were background corrected using a 7th order polynomial fitting algorithm (Mathworks MATLAB)[37] and vertically offset for clarity.

As expected,[23,24] the characteristic PTFE band at 734 cm^{-1} is not readily observed in any of the zero-offset spectra giving a poor S/N ratio of 1.7, 1.5 and 1.9 for the antler, metacarpal and bulla, respectively. Upon moving to a SORS collection geometry improved signal recovery of the buried PTFE layer is achieved as indicated by the spectra taken at 9 mm offset (see Fig. 1) showing S/N ratios of the 734 cm^{-1} PTFE band of 5.4, 3.5 and 3.7 for antler, metacarpal and bulla, respectively.

3.3 PTFE signal recovery dependence on spatial offset for variable PTFE depth

The PTFE-to-bone Raman intensity ratios were calculated for all spatial offsets and for all investigated depths (*i.e.* each position in the 'stack'). Representative results are shown in Fig. 2. At a depth of 1.0–1.4 mm the PTFE-to-bone ratio increases with SORS offset up until a maximum point and then decreases. The maximum PTFE-to-bone ratio is higher (0.55) for antler than it is for metacarpal and bulla (0.23 and 0.16) respectively and the offset at which the maximum occurs is lower for antler (2 mm) than it is for the other two (4 mm metacarpal and 4.5 mm bulla). This indicates that it is easier to recover signal from depths in less mineralized bones and that best signal recovery in more mineralized bones requires larger spatial offsets. For antler, however, these results should be seen in the context of its higher porosity compared to metacarpal and bulla.

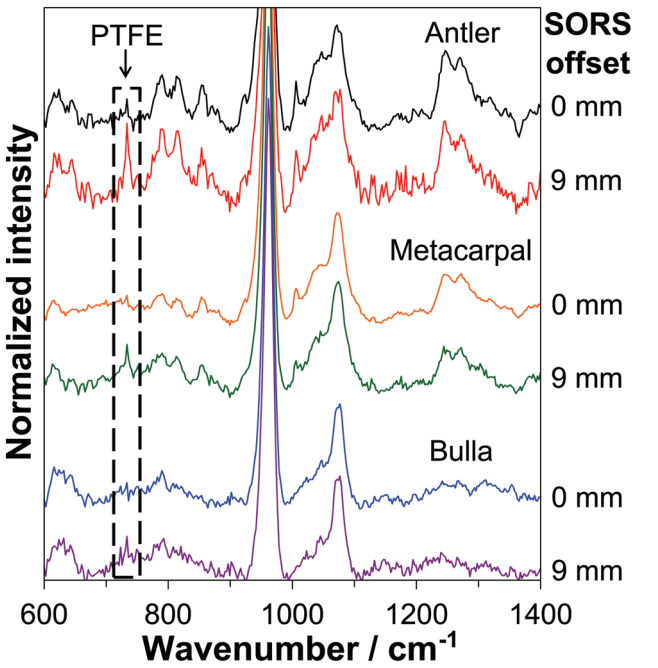

Fig. 1 Background-corrected Raman spectra (normalized to the bone phosphate band intensity at 961 cm^{-1}) of deer antler, equine metacarpal and whale bulla with a PTFE layer located below 4.0–4.2 mm of bone and with a bone segment placed beneath the stack. The spectra are displayed for spatial offsets of 0 mm and 9 mm and are vertically offset for clarity.

Fig. 2(b) shows the results from placing the PTFE layer at a greater depth of 3.0–3.3 mm. As would be expected the PTFE-to-bone ratio is lower compared to the smaller PTFE depth presented in Fig. 2(a) (by a factor of 3.2 for antler, 2.6 for metacarpal and 2.0 for bulla). The curve profiles for the two selected PTFE depths show different behavior, at 3 mm a monotonic increase contrasts with an increase in value to a maximum and then a decrease as the SORS offset is enlarged. However, in both cases the antler bone returns the greater PTFE signal recovery compared to the metacarpal or bulla, most likely due to a combination of its lower mineralization and higher porosity.

3.4 Major sampling depth inside bone

From the data presented in Fig. 2(a and b) it is possible to determine the optimum SORS offset yielding the maximum

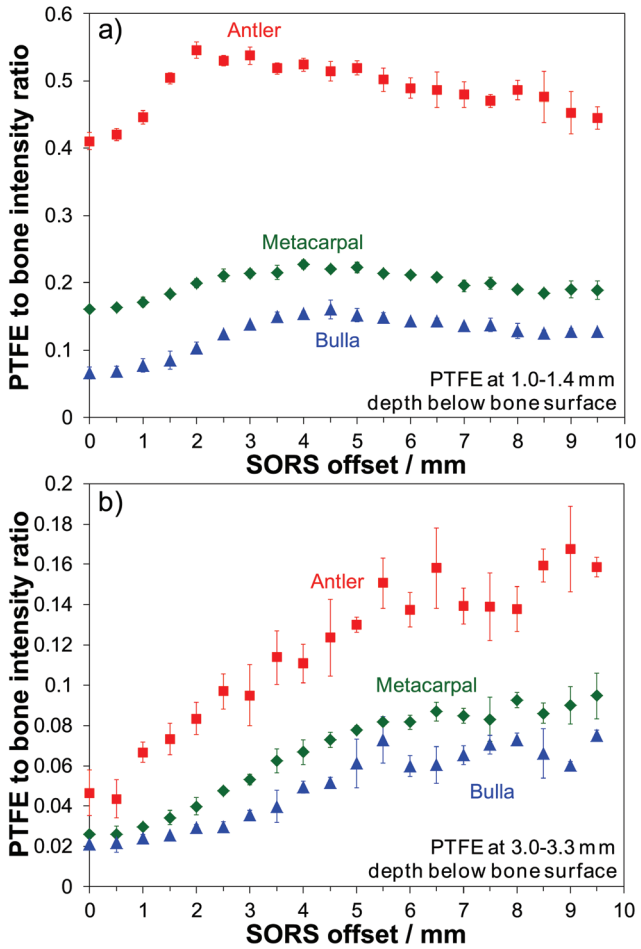

Fig. 2 PTFE to bone Raman intensity ratio dependence on SORS offset for deer antler, equine metacarpal and whale bulla; (a) PTFE at depth of 1.0–1.4 mm, (b) PTFE at depth of 3.0–3.3 mm.

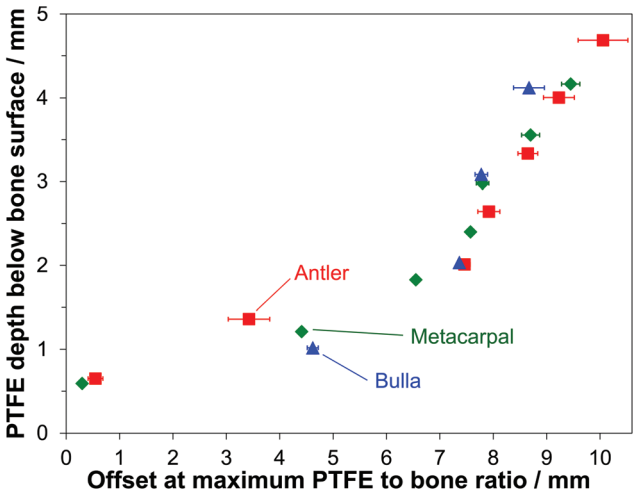

Fig. 3 SORS offsets giving maximum PTFE to bone ratio for selected PTFE depths below the bone surface determined for deer antler, equine metacarpal and whale bulla.

PTFE to bone intensity ratio. Importantly, provided that *a priori* information about the level of mineralization and porosity of the specimen are known, this permits one to estimate the approximate depth from which the major Raman signal contribution is collected for a given spatial offset within exposed bone during SORS measurements. Fig. 3 shows which offset gives the maximum signal for a specified depth. In line with our previous investigations on equine metacarpal[23] it is clear that the deeper the target (in this case the PTFE) is located within the bone the larger the SORS offset is needed to probe it effectively. The present data extends this earlier measurement and demonstrates that the depth of Raman signals collected from for a chosen SORS offset also depends on the level of bone mineralization. Taking a spatial offset of *ca.* 4 mm as an example, the major signal was recovered from depths of 1.4 mm, 1.2 mm and 1.0 mm for antler, metacarpal and bulla, respectively. In summary, it requires a greater SORS offset to reach material that is less than 2 mm from the surface in more mineralized bone.

Interestingly, it is the opposite for depths larger than 2 mm. In the case of 8 mm spatial-offset for example, the major signal contribution could be retrieved from depths of 2.6 mm for antler, 3.0 mm for metacarpal and 3.1 mm for bulla. This effect could indicate mineralization-specific differences in photon penetration properties (*i.e.* getting light beyond the surface) and photon propagation properties. For effective sampling at large depths (*i.e.* ≥4 mm) SORS offsets between 8.5 mm and 9.5 mm are required for all investigated bone types. It should be noted that the values given in Fig. 3 represent those depths from which the major signal contribution arises rather than the largest accessible depth; which in turn is dependent on the S/N ratio of a Raman band of the target substance.

3.5 Maximum accessible depth for signal recovery

Fig. 4 displays the S/N ratios of the prominent PTFE band at 734 cm^{-1} at different depths and for two selected SORS offsets. The largest S/N ratios being achieved with zero-offset and the PTFE layer at the surface. The ratios determined at 0 mm offset quickly decrease with increasing depth of the PTFE layer; the reduction for the largest investigated depths are by factors of 85, 106 and 34 for antler, metacarpal and bulla, respectively.

When the PTFE slice is placed at the bone material surface, *i.e.* on top of the stack of bone slices, and an offset of 9 mm is used the overlap of the PTFE target layer and the probed volume is minimal. With the PTFE moved deeper into the bone tissue the overlap will increase as well as the S/N ratio. However, this increase is accompanied by a general reduction in the total number of Raman photons recovered. Combining these two effects leads to results given in Fig. 4 (dashed lines). At a fixed offset of 9 mm, the reductions in S/N ratios going from zero depth of the PTFE layer, *i.e.* if it is located on top of the stack of bone slices, down to the largest investigated depths is by factors of 4.6 for antler, 6.2 for metacarpal and 2.2 for bulla.

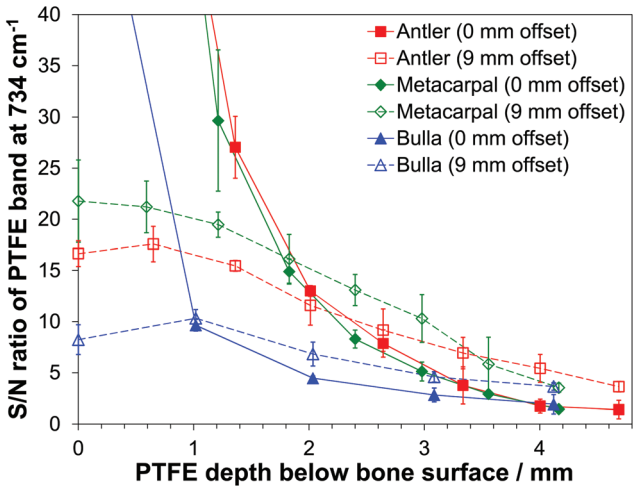

Fig. 4 PTFE S/N ratios as a function of bone layer thickness above the PTFE slice for spatial offsets of 0 mm and 9 mm using bone slices of deer antler, equine metacarpal and whale bulla. The lines are only drawn to guide the eye.

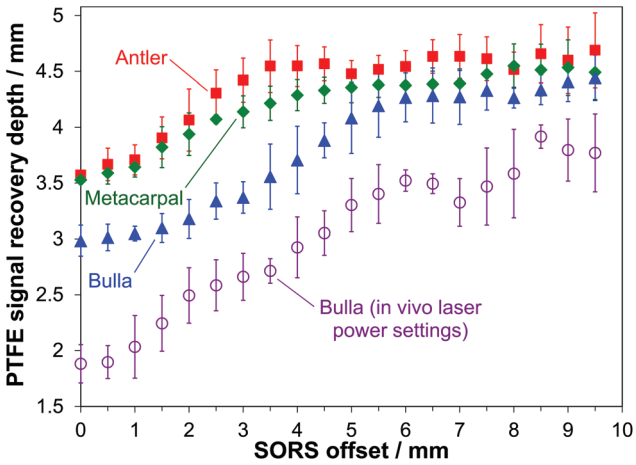

Fig. 5 Calculated signal recovery depths based on the 3-sigma criterion for deer antler, equine metacarpal and whale bulla (*ex vivo* laser power settings: I = 0.52–3.41 W cm^{-2}, depending on SORS offset), and for whale bulla using *in vivo* ($I \leq 0.36$ W cm^{-2}) laser power settings. All data underwent smoothing by a 3-point moving average.

The data presented in Fig. 4 suggests that there exists a specific depth for each bone where the S/N ratio is equal for zero and 9 mm offsets. This depth is dependent on the level of bone mineralization (as well as affected by porosity for the antler bone) and the corresponding values are 2.3 mm for antler, 1.8 mm for metacarpal and 1.0 mm for bulla. However, the majority of the signal collected always comes from the surface in the zero-offset case and, according to Fig. 3, from a depth of around 4 mm for spatial offsets of 9 mm.

In many cases, and especially in biomedical applications, there is a need to understand the maximum depth from which a given spectral signature can be detected. In the present study this signal recovery depth has been determined using the S/N ratios of the PTFE signal at 734 cm^{-1} and it was regarded to be detectable if its intensity equaled the threshold value of three times the noise level (3-sigma criterion). Fig. 5 (filled symbols) presents the results after smoothing by a 3-point moving average. For all bone types an overall increase in accessible depth is obtained with increasing SORS offset. There are however pronounced differences with respect to the bone mineralization level and the data shows evidence that 830 nm light can penetrate deeper into less mineralized bone tissue. In the case of the antler bone, however, this should be seen in the context of its higher porosity as well. As pointed out in our earlier study,[23] the signal recovery depth at zero spatial offset is much larger than those values achievable with confocal microscopy due to the significantly different excitation and collection geometries. At zero-offset depths of 3.6 mm, 3.5 mm and 3.0 mm can be reached for antler, metacarpal and bulla, respectively. This effect can be highly beneficial in investigations involving biological specimens because the large probed volume can effectively reduce sample heterogeneities.

The most pronounced increase in signal recovery depth takes place up to SORS offsets in the 4–5 mm range. Applying the largest spatial offsets (8.0 to 9.5 mm) gives the deepest signal recovery. In this way, Raman bands of substances not present in bone tissue can be detected up to depths of 4.7 mm for antler, 4.5 mm for metacarpal and 4.4 mm for bulla.

Potential clinical applications include the detection of characteristic Raman bands associated with the presence of pathological minerals due to early stage bone infection of diabetic patients that are not present in healthy bone tissue.[38,39] It is interesting to see that the demonstrated signal recovery depths in this study applying conventional SORS (*i.e.* without any signal enhancement effects in place) are more than half the distances achievable with surface-enhanced SORS (SESORS).[40] In the latter case, due to the involvement of metal nanoparticles for strong signal enhancement, depths of up to about 8 mm in bone have been demonstrated.[41]

3.6 Dependence of signal recovery depth on laser power

To assess a potential power dependence of photon migration effects the investigations have been repeated for whale bulla under identical experimental settings but with the laser power reduced to levels for skin-safe illumination (maximum permissible exposure level) according to BS EN 60825-1, *i.e.* not exceeding power densities of 0.36 W m^{-2}.

At the lower laser power the major sampling depth is virtually identical to the data presented in Fig. 3 (data not shown). However, there are pronounced differences in the maximum achievable depths for signal recovery as displayed in Fig. 5 (open circles). Using large spatial offsets around 9 mm maximum accessible depths inside the bone tissue of about 3.8 mm can be achieved. Compared to the *ex vivo* data (filled triangles in Fig. 5) these depths are on average reduced by 0.8 mm when using the permitted *in vivo* laser power levels.

These results indicate that the depth from which the main signal is collected does not show a pronounced difference with regards to the applied laser power in the range of powers used. For a given spatial offset, injecting a larger number of photons into the bone tissue does not move the *major* signal collection depth deeper into the bone. Nevertheless, as the overall number of photons is significantly reduced in the *in vivo* mode the likelihood of photons travelling into larger depths is reduced as well. As overall Raman signal intensity levels are smaller using *in vivo* laser power settings, the *maximum* depth for signal recovery according to the 3-sigma criterion is decreased in this case. It is noteworthy that the above defined probed volume inside the bone can be adjusted by two independent parameters, the spatial offset and the laser power. Up to the point where the effect of photon loss to the sides of the sample prevents photon migration back to the detector an increased laser power (*e.g.* in compliance with the new laser class 1C as introduced in BS EN 60825-1:2014) is therefore expected to enable the recovery of signals from larger depths.

4. Conclusion

This study provides valuable information about photon migration and the depth Raman signals are recovered from within selected bones of different mineralization. At depths of less than 2 mm clear differences between the selected types of bone have been observed. The underlying effects are not yet fully understood but the results indicate that photons can more easily migrate inside less mineralized bone tissue. At greater depths, we found that probing at the same depth inside the sample requires a slightly smaller SORS offset for more mineralized bone tissue. However, in the case of antler the higher porosity compared to metacarpal and bulla may also contribute to the observed effects.

The maximum accessible sampling depth was found to be dependent on the bone mineralization level as well. Raman signals not present in healthy bone tissue could successfully be recovered down to depths of 4.4–4.7 mm with the larger figure being from the less mineralized bone. It should be noted that this result may be not only due to the mineral content but partially be caused by the higher porosity of the antler as well. Applying safe laser illumination levels compatible with *in vivo* applications, even in the dense and highly mineralized bulla depths of up to 3.8 mm are still accessible. These results demonstrate the great potential of SORS for non-invasive screening of bone for the presence of infection, degeneration or cancer lesions deep inside bone matrix to determine their presence and nature or cancer margins, *e.g.* in the operating theatre where exposed bones are accessible.

Conflicts of interest

There are no conflicts of interest to declare.

Acknowledgements

The authors wish to thank the Engineering and Physical Sciences Research Council (EP/H002693/1), the Science and Technology Facilities Council, the Royal National Orthopaedic Hospital, and University College London for their support. We thank Prof. John Currey for providing the whale bone samples used in this study.

References

1 K. Buckley and P. Matousek, *Analyst*, 2011, **136**, 3039–3050.
2 P. Matousek, *Appl. Spectrosc.*, 2006, **60**, 1341–1347.
3 Z. Wang, H. Ding, G. Lu and X. Bi, *Opt. Lett.*, 2014, **39**, 3790–3793.
4 Z. Liao, F. Sinjab, G. Gibson, M. Padgett and I. Notingher, *Opt. Express*, 2016, **24**, 12701–12712.
5 P. Matousek and N. Stone, *Chem. Soc. Rev.*, 2016, **45**, 1794–1802.
6 K. Buckley, C. G. Atkins, D. Chen, H. G. Schulze, D. V. Devine, M. W. Blades and R. F. B. Turner, *Analyst*, 2016, **141**, 1678–1685.
7 S. L. Jacques, *Phys. Med. Biol.*, 2013, **58**, R37–R61.
8 A. Ghita, P. Matousek and N. Stone, *Analyst*, 2016, **141**, 5738–5746.
9 M. D. Keller, S. K. Majumder and A. Mahadevan-Jansen, *Opt. Lett.*, 2009, **34**, 926–928.
10 M. D. Keller, E. Vargis, N. de Matos Granja, R. H. Wilson, M.-A. Mycek, M. C. Kelley and A. Mahadevan-Jansen, *J. Biomed. Opt.*, 2011, **16**, 077006.
11 Z. Liao, F. Sinjab, A. Nommeots-Nomm, J. Jones, L. Ruiz-Cantu, J. Yang, F. Rose and I. Notingher, *Anal. Chem.*, 2017, **89**, 847–853.
12 H. Ding, G. Lu, C. West, G. Gogola, J. Kellam, C. Ambrose and X. Bi, *Proc. SPIE*, 2016, **9689**, 96894M.
13 P. I. Okagbare, D. Begun, M. Tecklenburg, A. Awonusi, S. A. Goldstein and M. D. Morris, *J. Biomed. Opt.*, 2012, **17**, 090502.
14 P. Matousek and N. Stone, *J. Biophotonics*, 2013, **6**, 7–19.
15 K. Buckley, J. G. Kerns, J. Vinton, P. D. Gikas, C. Smith, A. W. Parker, P. Matousek and A. E. Goodship, *J. Raman Spectrosc.*, 2015, **46**, 610–618.
16 J. R. Peterson, P. I. Okagbare, S. De La Rosa, K. E. Cilwa, J. E. Perosky, O. N. Eboda, A. Donneys, G. L. Su, S. R. Buchman, P. S. Cederna, S. C. Wang, K. M. Kozloff, M. D. Morris and B. Levi, *Bone*, 2013, **54**, 28–34.
17 M. V. Schulmerich, K. A. Dooley, T. M. Vanasse, S. A. Goldstein and M. D. Morris, *Appl. Spectrosc.*, 2007, **61**, 671–678.
18 M. V. Schulmerich, J. H. Cole, J. M. Kreider, F. Esmonde-White, K. A. Dooley, S. A. Goldstein and M. D. Morris, *Appl. Spectrosc.*, 2009, **63**, 286–295.
19 J.-L. H. Demers, F. W. L. Esmonde-White, K. A. Esmonde-White, M. D. Morris and B. W. Pogue, *Biomed. Opt. Express*, 2015, **6**, 793–806.

20 K. Buckley, J. G. Kerns, A. W. Parker, A. E. Goodship and P. Matousek, *J. Raman Spectrosc.*, 2014, **45**, 188–192.
21 K. Buckley, J. G. Kerns, P. D. Gikas, H. L. Birch, J. Vinton, R. Keen, A. W. Parker, P. Matousek and A. E. Goodship, *IBMS BoneKEy*, 2014, **11**, 602.
22 K. Sowoidnich, J. H. Churchwell, K. Buckley, J. G. Kerns, A. E. Goodship, A. W. Parker and P. Matousek, *Proc. SPIE*, 2015, **9540**, 954009.
23 K. Sowoidnich, J. H. Churchwell, K. Buckley, A. E. Goodship, A. W. Parker and P. Matousek, *J. Raman Spectrosc.*, 2016, **47**, 240–247.
24 K. Sowoidnich, J. H. Churchwell, K. Buckley, J. G. Kerns, A. E. Goodship, A. W. Parker and P. Matousek, *Proc. SPIE*, 2016, **9887**, 988719.
25 K. Buckley, J. G. Kerns, H. L. Birch, P. D. Gikas, A. W. Parker, P. Matousek and A. E. Goodship, *J. Biomed. Opt.*, 2014, **19**, 111602.
26 P. Zioupos, J. D. Currey and A. Casinos, *Connect. Tissue Res.*, 2000, **41**, 229–248.
27 M. V. Schulmerich, K. A. Dooley, M. D. Morris, T. M. Vanasse and S. A. Goldstein, *J. Biomed. Opt.*, 2006, **11**, 060502.
28 K. Buckley, P. Matousek, A. W. Parker and A. E. Goodship, *J. Raman Spectrosc.*, 2012, **43**, 1237–1243.
29 J. Mihály, S. Sterkel, H. M. Ortner, L. Kocsis, L. Hajba, É. Furdyga and J. Mink, *Croat. Chem. Acta*, 2006, **79**, 497–501.
30 J. D. Currey, *J. Biomech.*, 1979, **12**, 313–319.
31 R. D. Bloebaum, J. G. Skedros, E. G. Vajda, K. N. Bachus and B. R. Constantz, *Bone*, 1997, **20**, 485–490.
32 J. D. Currey, *J. Biomech.*, 1988, **21**, 131–139.
33 T. Landete-Castillejos, J. D. Currey, F. Ceacero, A. J. García, L. Gallego and S. Gomez, *Bone*, 2012, **50**, 245–254.
34 P.-Y. Chen, A. G. Stokes and J. McKittrick, *Acta Biomater.*, 2009, **5**, 693–706.
35 S. Lees, J. M. Ahern and M. Leonard, *J. Acoust. Soc. Am.*, 1983, **74**, 28–33.
36 S. Gomez, A. J. Garcia, S. Luna, U. Kierdorf, H. Kierdorf, L. Gallego and T. Landete-Castillejos, *Bone*, 2013, **52**, 506–515.
37 C. A. Lieber and A. Mahadevan-Jansen, *Appl. Spectrosc.*, 2003, **57**, 1363–1367.
38 K. A. Esmonde-White, F. W. Esmonde-White, C. Holmes, M. D. Morris and B. Roessler, *Trans. Orthop. Res. Soc.*, 2012, **37**, 909.
39 K. A. Esmonde-White, F. W. Esmonde-White, C. M. Holmes, M. D. Morris and B. J. Roessler, *Diabetes Care*, 2013, **36**, 3652–3654.
40 N. Stone, K. Faulds, D. Graham and P. Matousek, *Anal. Chem.*, 2010, **82**, 3969–3973.
41 B. Sharma, K. Ma, M. R. Glucksberg and R. P. Van Duyne, *J. Am. Chem. Soc.*, 2013, **135**, 17290–17293.